WORLD CONFERENCE ON TIMBER ENGINEERING 2025
BRISBANE, AUSTRALIA

Advancing Timber for the Future Built Environment

EXPERIMENTAL AND ANALYTICAL INVESTIGATION OF A NOVEL ADHESIVE-FREE TIMBER-STEEL COMPOSITE USING EUCALYPTUS GLOBULUS HARDWOOD.

Richard Nero[1], Philip Christopher[2], and Tuan Ngo[3]

ABSTRACT: The objective of this study is to investigate the structural behaviour of a novel adhesive-free timber-steel composite (AFTSC) system as a high-performance floor panel for sustainable mid- and high-rise construction. Local plantation eucalyptus globulus timber boards and laser cut mild-steel were used to fabricate the test specimens. Four-point bending tests were carried out to experimentally record the force, displacement, and failure mechanism of the panels. An analytical model was generated and compared against the experimental results. The novel AFTSC panels maintained near full composite action past 40% of ultimate load and consistently exhibited substantial ductile behaviour. In addition, the effective ultimate bending capacity of the timber components was found to increase by up to 25% when included in the AFTSC panels. This demonstrates the high-performance credentials of the novel AFTSC system along with the potential to valorise plantation hardwoods such as eucalyptus globulus.

KEYWORDS: composite, experimental, adhesive-free, four-point bending, ductility

1 – INTRODUCTION

1.1 BACKGROUND

Concern about the petrochemicals in the adhesives used in manufacturing impede the recyclability of these conventional EWPs, and along with the volatile organic compounds (VOCs) emitted over their lifespan has given rise to research into adhesive-free alternatives [1], [2]. Innovations such as dowel laminated timber (DLT), cross-laminated timber (CLT) panels using hardwood dowels, and timber-timber hollow-core panels have been shown to be viable adhesive-free alternatives [2], [3], [4], [5], [6], [7], [8].

Reinforcing timber with steel has also been explored to enhance the bending stiffness, bending strength, and ductility of timber members. The inclusion of reinforcement in the tension zone increases the effective bending stiffness, redistributes bending stresses to reduce tension face stress while increasing compression face stress, and initiates flexural failure in the compression face, typically resulting in a ductile failure mode [9], [10], [11], [12], [13], [14], [15], [16]. While there are numerous examples of timber-steel composite systems using adhesives [10], [12], [13], [14], [15], [16], adhesive-free systems are relatively limited [9], [11]. Although previous studies investigating an adhesive-free steel-reinforced beam did report bending stiffness increased by 34% over a timber-only beam, the proposed system did not overcome the dimensional limitations of the component boards. This research work focuses on the development of an adhesive-free timber-steel composite (AFTSC) floor panel made from sustainably harvested plantation eucalyptus globulus (southern blue gum). The AFTSC panel aims to serve as an adhesive-free alternative to existing steel-reinforced timber products, as well as a dimensionally flexible and high-performance version of the current NLT and DLT systems.

1.2 DESCRIPTION OF THE SYSTEM

The novel AFTSC system developed and experimentally tested in this study consists of three components. An isometric view of the build-up is shown in Figure 1.The top component (A) is formed from individual timber boards nailed together and oriented edgewise. The middle component (B) is a series of

[1] Richard Nero, Department of Infrastructure Engineering, University of Melbourne, Melbourne, Australia, richard.nero@unimelb.edu.au
[2] Philip Christopher, Department of Infrastructure Engineering, University of Melbourne, Melbourne, Australia, pbc@unimelb.edu.au
[3] Tuan Ngo, Department of Infrastructure Engineering, University of Melbourne, Melbourne, Australia, dtngo@unimelb.edu.au

 https://doi.org/10.52202/080513-0307

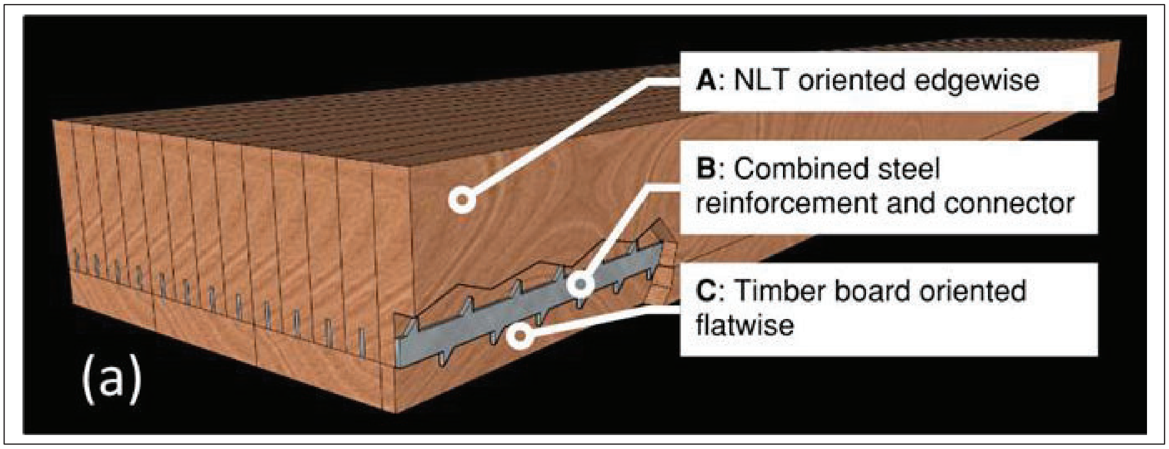

Figure 1. Schematic of the novel AFTSC showing the three components.

toothed steel bars that function as both reinforcement and connectors. The bottom component (C) is made up of additional timber boards oriented flatwise. The toothed steel bars are positioned at the interface between components A and C and resist the bending-induced shear slip between those components. As the shear stresses push component A over and past component C the shape and direction of the teeth provide a series of bearing surfaces to resist that movement. Component B is located in the lower half of the system to increase the effective bending stiffness when exposed to conventional sagging moments.

The shape of the steel component is designed to predominantly resist horizontal rather than vertical movement between the components and so functions differently to the conventional nail or screw fixings in other composite timber products. Vertical movement or separation is resisted partly by the gravitational forces from the self-weight and other deadloads effectively clamping the components together, and partially by the teeth acting like a double-sided nail-plate. The inclusion of the bottom timber layer provides a protective char layer in a fire scenario, shielding the steel reinforcement. By allowing for the addition of discrete timber layers the proposed system overcomes the dimensional limitations of edgewise-oriented DLT while retaining the high stiffness characteristics.

1.3 AIMS OF THE STUDY

The primary aim of this study is to experimentally evaluate the bending strength, stiffness, and ductility of the AFTSCs to validate their structural performance.

2 MATERIALS AND METHODOLOGY

2.1 MANUFACTURING PROCESS

The stages of the manufacturing process are show in Figure 2.

1. Sawn timber boards are sequentially stacked, clamped, and nailed together to form a solid NLT panel. All minor instances of bow, flex or warping are removed by pre-nail clamping.
2. The NLT panel is then oriented edgewise and has 3mm wide by 15mm deep grooves cut into the middle of each of the component timber boards. This groove will house the depth of the continuous section of the reinforcing steel bar.
3. The laser cut toothed steel bars are inserted into the grooves in the NLT and then have an additional timber board laid flatwise on top.
4. Sequential pressing of up to 8 MPa along the length of the panels progressively forces the teeth of the steel bars into the NLT and flatwise timber boards. This process dislodges and compresses the timber fibres rather than severing them.

Three panels were manufactured for the experimental four-point bending tests in this study. The number of boards and dimensions of each panel are summarised in Table 1. The steel reinforcement was laser cut from a hot rolled 3 mm thick grade HA350 steel plate. The steel was graded to AS/NZS 1594 [17] and achieved an upper yield strength prior to the first decrease in force (ReH) of 415 MPa tested in accordance with AS 1391 [18]. The reported density and elastic modulus of the steel were 7850 kg/m3 and 210 GPa, respectively.

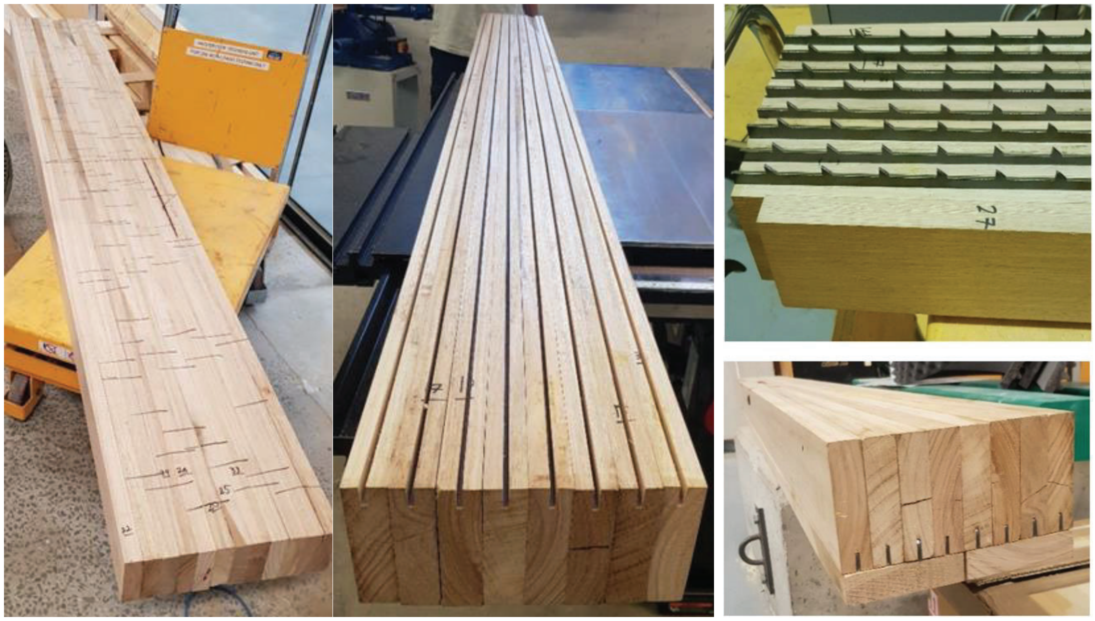

Figure 2. Manufacturing and assembly process for the AFTSCs (clockwise from left, steps 1, 2, 3, and 4).

Table 1. AFTSC panel dimensions.

Panel label		P1	P2	P3
Number of boards, $\boldsymbol{n}$	[#]	5	10	15
Width, $\boldsymbol{b}$	[mm]	100	200	300
Length, $\boldsymbol{L_{total}}$	[mm]	2200	2200	2200
Span, $\boldsymbol{L}$	[mm]	2150	2150	2150
Depth, $\boldsymbol{d}$	[mm]	125	125	125

2.2 FOUR-POINT BENDING TESTS

Four-point bending tests were conducted on the three panels described in Table 1. The depth of 125 mm and span of 2150 mm was consistent across all panels. Load was applied to the panels via a 500 kN vertically mounted MTS displacement-controlled actuator. The midspan deflection measurements were recorded with a ILD 1420-100 laser sensor. The load heads were located six times the panel depth (750 mm) in from each support. The four-point bending setup is shown in Figure 3. Each specimen was loaded to approximately 40% of the estimated failure load then un-loaded over three cycles before being loaded to failure. The initial three ramps were used to ensure any slack within the test system was removed before a stiffness measurement was made, as well as to observe whether any plastic deformation occurred before 40% of ultimate load.

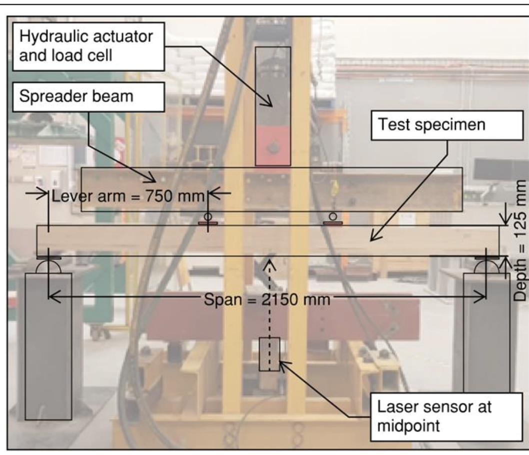

Figure 3. Four-point bending test setup.

The experimentally measured system stiffness per metre width (EI_{exp}) was calculated as a function of the lever arm (a), the span (L), the width (b), and the force-displacement gradient ($\frac{\Delta F}{\Delta e}$).

$$EI_{exp} = \left[\left(\frac{3 \cdot a}{4 \cdot L}\right) - \left(\frac{a}{L}\right)^3\right] \cdot \frac{\mathrm{L}^3}{12} \cdot \left(\frac{\Delta F}{\Delta e}\right) \cdot \frac{1000}{b} \quad (1)$$

The slip modulus (K_i) of the shear interface between both timber-steel and steel-timber was calculated according to composite beam theory. The Gamma method presented in Eurocode 5 Annex B [19] was used to relate the measured effective system stiffness (EI_{eff}) to a Gamma value (γ_i). The Gamma value (γ_i) is a function of the elastic modulus (E_i), area (A_i), and span (L) of the system as well as the spacing (s_i) and slip modulus (K_i) of the fixings.

https://doi.org/10.52202/080513-0307

$$EI_{eff} = \sum E_i \cdot I_i + \gamma_i \cdot E_i \cdot A_i \cdot {z_i}^2 \tag{2}$$

$$\gamma_i = \left[1 + \frac{\pi^2 \cdot E_i \cdot A_i \cdot s_i}{K_i \cdot L^2}\right]^{-1} \tag{3}$$

As the slip modulus of the interface between components in the system decreases the gamma value also decreases. This in turn reduces the effective stiffness of the section as the system performs with less than 100% composite action. As composite action reduces, the neutral axis (NA) for each of the component layers shifts to align closer to their respective local neutral axes. This intermediate NA is termed $y_{i,0}$ and is assumed to vary linearly between the NA of the full composite system when $\gamma_i = 1$, and the local NA ($y_{i,NA}$) as $\gamma_i \to 0$. As the effective NA position changes the degree and direction of the stresses in each component also changes. Equations (4)–(7) step through the analytical approach adopted in this study for calculating the normal and shear stresses in each component of the system. The normal stress (σ_j) at height y_j in the cross-section is a function of the acting moment (M), the effective component NA ($y_{i,0}$), the effective section modulus of the system (I_{eff}), and the ratio between the MoE of the component in question and the nominal MoE of the system (η_i).

$$\sigma_j = \frac{M \cdot |y_{i,0} - y_j|}{I_{eff}} \cdot \eta_i \tag{4}$$

$$y_{i,0} = \gamma_i \cdot \frac{\sum \gamma_i \cdot E_i \cdot A_i \cdot y_i}{\sum \gamma_i \cdot E_i \cdot A_i} + (1 - \gamma_i) \cdot y_{i,NA} \tag{5}$$

$$I_{eff} = \frac{EI_{eff}}{E_{nom}} \tag{6}$$

$$\eta_i = \frac{E_i}{E_{nom}} \tag{7}$$

The shear stress (τ_j) up the height of the cross-section is similarly a function of the acting shear force (V), first moment of area (Q_j), the effective section modulus of the system (I_{eff}) and the width (b_i). A_j is the area of the system that is at or above height j and $\overline{y_j}$ is the distance between the effective NA of component i ($y_{i,0}$) and the NA of component i above height j ($y_{i,j}$).

$$\tau_j = \frac{V \cdot Q_j}{I_{eff} \cdot b_i} \tag{8}$$

$$Q_j = A_j \cdot \overline{y_j} \tag{9}$$

$$\overline{y_j} = |y_{i,0} - y_{i,j}| \tag{10}$$

$$y_{i,j} = \gamma_i \cdot \frac{\sum \gamma_i \cdot E_i \cdot A_{i,j} \cdot y_{i,j}}{\sum \gamma_i \cdot E_i \cdot A_{i,j}} + (1 - \gamma_i) \cdot y_{i,NA} \tag{11}$$

$A_{i,j}$ is the area of the component i that is at or above height j. The NA of component i above height j is termed $y_{i,j}$ and is calculated similarly to the effective component NA ($y_{i,0}$). The difference is that it only considers the area at or above a certain height j, as is the conventional approach to shear calculations.

Ductility, in the context of a beam in flexure, is the capacity for a system to maintain post-yield plastic deformation without a reduction in load. Ductility is an important metric when considering the effective robustness of a system since it provides a visual warning of the impending collapse of a structure as well as energy dissipation in an extreme event. A quantitative measure of ductility is often considered as either a function of the deflections at yield (Δ_{yield}) and ultimate failure (Δ_{max}) or a function of the energy absorbed in total (W_{tot}) and within the elastic zone (W_{elas}).

$$D_d = \frac{\Delta_{max}}{\Delta_{yield}} \tag{12}$$

$$D_e = 0.5 \cdot \left(\frac{W_{tot}}{W_{elas}} + 1\right) \tag{13}$$

3 RESULTS AND DISCUSSION

This section presents the findings of the experimental AFTSC panel bending tests and analytical prediction model. The measured ductility is then calculated using both deflection- and energy-based approaches and the performance improvements of the AFTSC panels are quantified.

3.1 EXPERIMENTAL RESULTS

The force-displacement relationships of the AFTSC panels in four-point bending are presented in Figure 4. All three panels had the same depth and span, but varying widths. The plot shows the consistency of the behaviour across all three specimens. There are two clear linear-elastic regions followed by a plastic plateauing of the forces which are then maintained with further substantial deflections before ultimate failure. No large drops in force are observed until close to the end of each of the plastic deformation regions.

A focused evaluation of the final ramp loading panel P1 to failure can be seen in Figure 5. The two y-axes describe firstly the force on the left-hand side, and

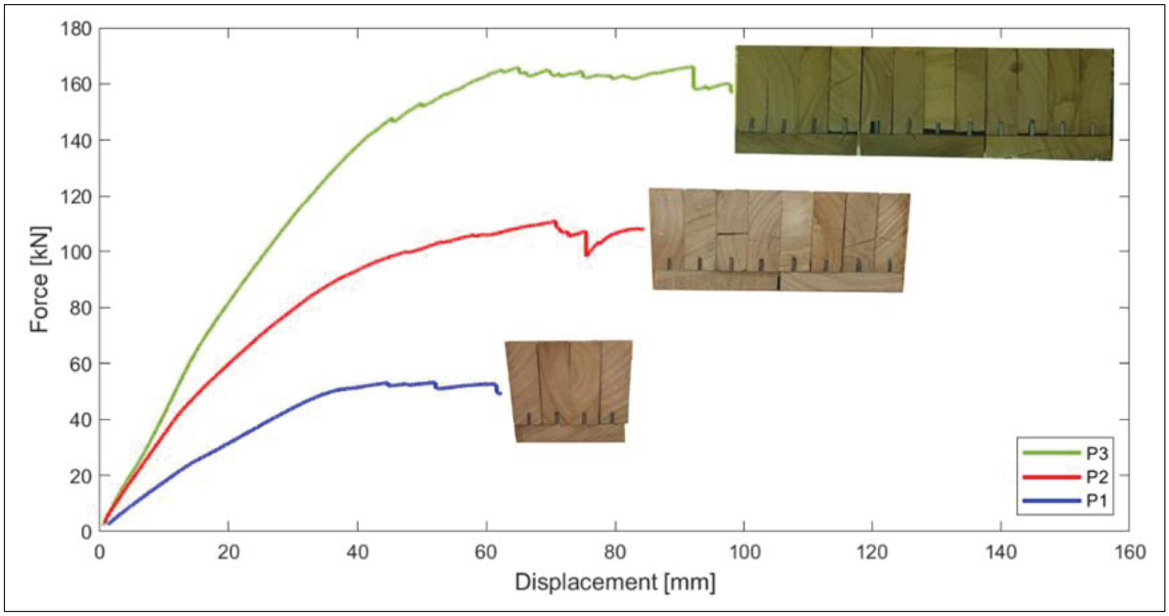

Figure 4. Force-displacement relationships of each of the three AFTSC panels; P1, P2, and P3 alongside images of their respective cross-sections.

secondly the rate of change of the force over the displacement (i.e.: the member stiffness) on the right-hand side. The member stiffness-displacement is an important relationship to consider as experimental observations identified a distinct step between two linear-elastic regions of the force-displacement curve. This step occurs at 25, 46, and 58 kN, equivalent to 47%, 42%, and 35% of the ultimate load for panels P1, P2, and P3, respectively. The step marks a change in effective member stiffness of the panels down from the initial stiffnesses of 1.7, 3.3, and 4.5 kN/mm, respectively. This initial member stiffness was equivalent to 99%, 97%, and 90% of the predicted effective composite action for the panels P1, P2, and P3, respectively. The dashed line describes the average measured stiffness before and after the step. Rationalising the stiffness measurements to discrete values enables the calculation of two distinct slip moduli for the curve. This in turn allows the analytical model to accurately describe the variable stiffness behaviour of the composite system.

The analytically modelled normal-stress, normal-strain, and shear-stress within the panel section P1 at each of the 4 positions are shown in Figure 6.The values before the step are shown in position 1 and after the step, in position 2. The shear stress in the interface between the layers of the panel was calculated at position 1 as 1.48, 1.35, and 1.20 MPa for panels P1, P2, and P3 respectively. This is the degree of shear stress that instigated a decrease in the effective slip modulus of the system and a change in the elastic stiffness.

The degree of effective composite action is illustrated in positions 2, 3, and 4 of Figure 6 by the departure from a single linear strain plot at the shear interfaces above and below the steel reinforcement; 25 and 40 mm on the y-axis. Position 3 (force-displacement in Figure 5 and stress and strain plots in Figure 6) marks the predicted end of the elastic zone based on the analytically modelled normal stress in the steel section reaching 415 MPa, which is the upper yield limit of the steel reinforcement. After this point the measured member stiffness can no longer be used to derive the slip modulus – and so degree of composite action – since further reduction in stiffness must be considered as a combination between slip and plastic material deformation of the steel. Experimental observations identified the rapid decrease in stiffness occurring concurrently with crushing of the timber fibres in the compression face. Position 4 marks the location of ultimate bending capacity after which tensile fractures in the timber in both the flatwise bottom boards and the tension zone of the edgewise boards result in permanent capacity loss and eventually ultimate member failure. The maximum compressive stress in the timber boards in the panel was recorded at position 4.

https://doi.org/10.52202/080513-0307

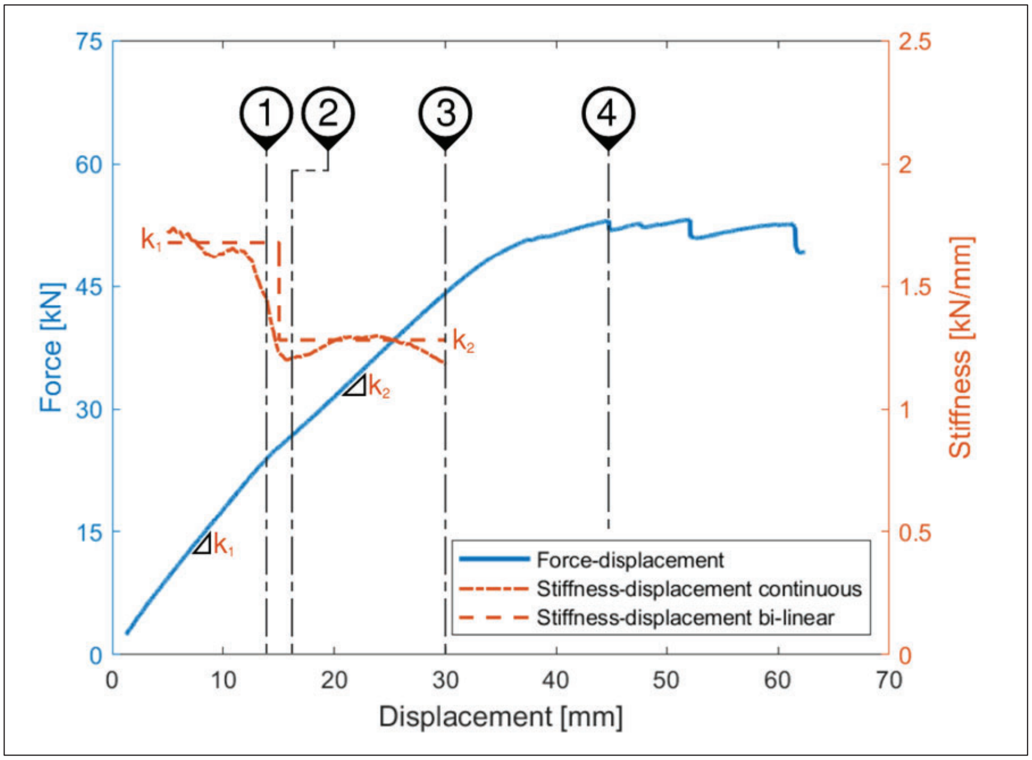

Figure 6. Relationship between force-displacement and flexural stiffness-displacement for panel P1 highlighting key positions.

The experimentally and analytically derived flexural characteristics of the three panel tests are summarised in Table 2. Both the effective system stiffness and the shear stress at the point of shear slip were observed to decrease with an increase in beam width. Although an insufficient number of tests were performed to confirm such a trend, it could be attributed to the increasing risk of manufacturing errors or inconsistencies that arise from manually assembling panels with additional components. This trend could be investigated further by manufacturing future panels in a more controlled and consistent industrial setting. The slip modulus for each panel was measured at position 2 directly after the observed step between the two linear-elastic stiffness regions and varied between 8.5 and 16.8 kN/mm. These measured values are of a similar magnitude to the slip

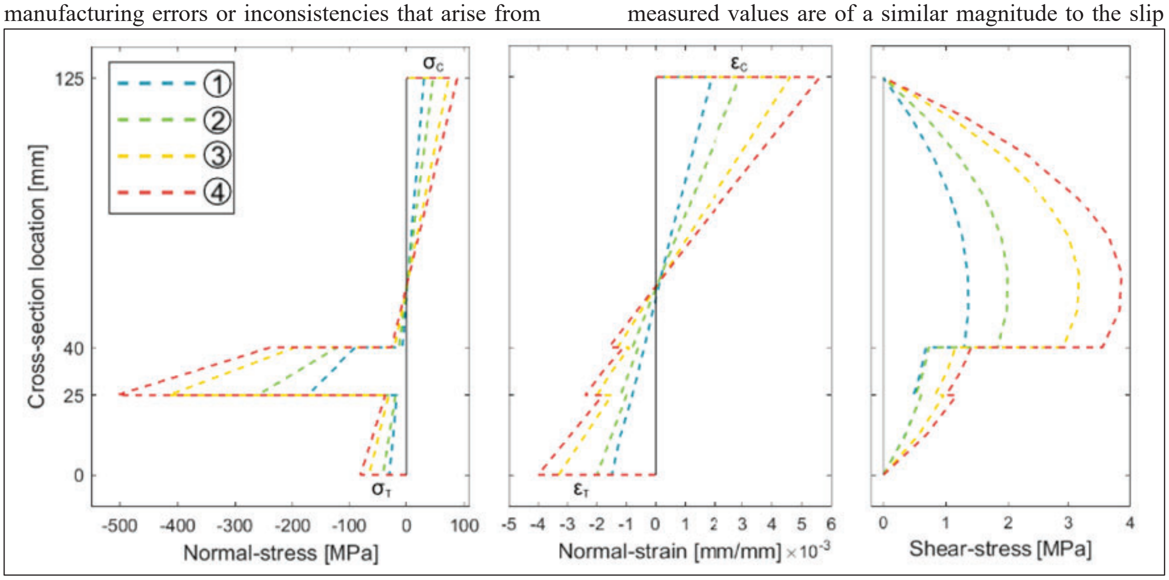

Figure 5. Analytically modelled normal stress, strain, and shear stress within the cross-section of panel P1 at key points as labelled in Figure 6.

moduli for self-tapping screw connections of between 5-25 kN/mm reported in the literature [20], [21], [22], [23]. The maximum bending stress capacity of the timber was calculated from the peak moment resisted by the system.

Table 2. Experimental and analytical flexural characteristics of the AFTSC panels measured from four-point bending tests.

Label		**P1**	**P2**	**P3**	**Avg**
Width	b [mm]	100	200	300	-
Member stiffness	k_{exp} [kN/mm]	1.7	3.3	4.5	-
System stiffness per metre width	EI_{exp} [Nmm2/m]	3.06 E+12	2.98 E+12	2.72 E+12	2.92 E+12
Shear stress at elastic change	τ_{timber} [MPa]	1.48	1.35	1.20	1.34
Slip modulus after elastic change	K_{slip} [kN/mm]	12.0	8.5	16.8	12.4
Max stress in timber	σ_{timber} [MPa]	90	114	108	104

Overall, the panels experimentally tested were relatively consistent. They exhibited high-performance in terms of initial flexural stiffness close to full composite action while maintaining high initial stiffness past 40% of ultimate load. High degrees of ductility where measured due to plastic yielding in both the steel reinforcement and compression face of the timber. Additionally, the panels were observed to remain intact after ultimate failure, without noticeable material shedding from fractures.

3.2 DUCTILITY

The final key performance metric investigated in this experimental study was ductility. This parameter is an important indication of robustness and measures the ability of the system to undergo plastic deformation without a loss of load.

The quantitative measures of the deflection-based and energy-based ductility for the AFTSC panels are presented in Table 3.

Table 3. Ductility measurements of AFTSC panels and timber feedstock.

Label		**P1**	**P2**	**P3**
Deflection at initial yield	Δ_{yield} [mm]	33.7	37.5	36.3
Deflection at ultimate failure	Δ_{max} [mm]	62.6	85.1	98.2
Energy at elastic limit	W_{elast} [J]	879	1946	2580
Energy total	W_{tot} [J]	2374	6870	12339
Ductility, deflection based	D_d [-]	1.86	2.27	2.71
Ductility, energy based	D_e [-]	1.85	2.27	2.89

The panels exhibited deformation-based ductility values of 1.86 to 2.71, and energy-based ductility values of 1.85 to 2.89. The observed ductility in the panels was a product of three factors. Initially the steel reinforcement reached its yield limit (position 3 in Figure 5) of approximately 415 MPa causing a reduction in flexural stiffness while the applied load continued to rise, albeit at a slower rate. The second contribution to the ductility was the top layer of edgewise timber boards which began crushing of the extreme compression fibres resulting in a further loss of stiffness and a plateauing of the applied load. The third source of ductility in the panels was the slip in the connection between the three layers. As the applied load increased and the shear stresses built up in the panel, the timber fibres in both the top and bottom layers began locally crushing at the location of the steel teeth. The extent of this local crushing was relatively minor due to the hardness of the E. globulus timber. This can be seen in Figure 7 where a section of the panel has been removed to reveal the extent of the fibre crushing at the connection during the post-yield ductile deformation. Additionally, the figure shows the plastic deformation of the steel reinforcement flat bar after being disassembled from the panel.

Figure 7. Section of an AFTSC panel post-failure showing the steel connection and the disassembled reinforcement.

https://doi.org/10.52202/080513-0307

4 CONCLUSIONS

In this study the behaviour and performance of a novel adhesive-free timber-steel composite (AFTSC) floor system was investigated through a combination of experimental tests and analytical modelling. The aim was to explore the flexural behaviour of the system, evaluating the bending strength, stiffness, and ductility.

Force-displacement relationships derived from four-point bending tests revealed two distinct linear elastic regions followed by post-yield plastic deformations and a plateauing load. The initial linear elastic region was maintained past 40% of ultimate load across all panels and achieved 95% effective composite action on average.

The local material strength of the timber in compression was the limiting factor at ultimate limit state failure, along with tensile yielding of the steel. This demonstrated the capability of the AFTSC system to improve the effective strength of the component timber boards by forcing them to yield according to their stronger local material properties rather than their weaker global material properties.

Further investigation is needed into the slip behaviour of the steel-timber interface including the impact of tooth arrangement, as well as experiments on larger-scale specimens investigating the long-term creep effects and fire performance. This further work will serve to inform a more accurate and complete analytical model while also enabling the optimisation of more materially efficient panels.

5 ACKNOWLEDGEMENT

This research was supported by funding from the Australian Government Research Training Program Scholarship (RTP). This research was partially supported through the ARC Discovery project DP210102499: Innovative composite systems with enhanced resilience to extreme loads. This research was partially supported by the Building 4.0 CRC, an industry-led research initiative co-funded by the Australian Government. The product is currently under patent review, Australian Provisional Application No 2024901726. The authors would also like to acknowledge and thank Dr Bernard Gibson and University of Melbourne research student Hugo Groot for their assistance with the experimental work.

6 REFERENCES

[1] Z. Guan et al., DEVELOPMENT OF ADHESIVE FREE ENGINEERED WOOD PRODUCTS – TOWARDS ADHESIVE FREE TIMBER BUILDINGS. 2018.

[2] I. El-Houjeyri et al., ‘Experimental investigations on adhesive free laminated oak timber beams and timber-to-timber joints assembled using thermo-mechanically compressed wood dowels’, Construction and Building Materials, vol. 222, pp. 288–299, Oct. 2019, doi: 10.1016/j.conbuildmat.2019.05.163.

[3] L. Han, A. Kutnar, J. Sandak, I. Šušteršič, and D. Sandberg, ‘Adhesive-and Metal-Free Assembly Techniques for Prefabricated Multi-Layer Engineered Wood Products: A Review on Wooden Connectors’, Forests, vol. 14, no. 2, Art. no. 2, Feb. 2023, doi: 10.3390/f14020311.

[4] V. Baño and G. Moltini, ‘Experimental and numerical analysis of novel adhesive-free structural floor panels (TTP) manufactured from timber-to-timber joints’, Journal of Building Engineering, vol. 35, p. 102065, Mar. 2021, doi: 10.1016/j.jobe.2020.102065.

[5] M. Derikvand, S. Hosseinzadeh, and G. Fink, ‘Mechanical Properties of Dowel Laminated Timber Beams with Connectors Made of Salvaged Wooden Materials’, Journal of Architectural Engineering, 2021, Accessed: Mar. 09, 2023. [Online]. Available: https://ascelibrary.org/doi/epdf/10.1061/%28ASCE%29AE.1943-5568.0000513

[6] X. Sun, M. He, and Z. Li, ‘Novel engineered wood and bamboo composites for structural applications: State-of-art of manufacturing technology and mechanical performance evaluation’, Construction and Building Materials, vol. 249, p. 118751, Jul. 2020, doi: 10.1016/j.conbuildmat.2020.118751.

[7] A. Sotayo et al., ‘Review of state of the art of dowel laminated timber members and densified wood materials as sustainable engineered wood products for construction and building applications’, Developments in the Built Environment, vol. 1, p. 100004, Feb. 2020, doi: 10.1016/j.dibe.2019.100004.

[8] W. Plowas, R. Hairstans, T. Bell, and J. Bros Williamson, ‘Understanding the compatibility of UK resource for dowel laminated timber construction’, Oct. 2016, Accessed: Aug. 11, 2022. [Online]. Available: https://napier-

repository.worktribe.com/output/169670/understanding-the-compatibility-of-uk-resource-for-dowel-laminated-timber-construction

[9] J. R. Hoyle, ‘Steel-reinforced wood beam design’, FPJ, vol. 25, no. 4, pp. 17–23, 1975.

[10] P. Dietsch and R. Brandner, ‘Self-tapping screws and threaded rods as reinforcement for structural timber elements – A state-of-the-art report’, Construction and Building Materials, vol. 97, pp. 78–89, Oct. 2015, doi: 10.1016/j.conbuildmat.2015.04.028.

[11] T. Nowak, J. Jasieńko, E. Kotwica, and S. Krzosek, ‘Strength enhancement of timber beams using steel plates–review and experimental tests’, Drewno: prace naukowe, doniesienia, komunikaty, vol. 59, 2016.

[12] R. Tomasi, M. A. Parisi, and M. Piazza, ‘Ductile design of glued-laminated timber beams’, Practice Periodical on Structural Design and Construction, vol. 14, no. 3, pp. 113–122, 2009.

[13] T. Ghanbari Ghazijahani, H. Jiao, and D. Holloway, ‘Composite timber beams strengthened by steel and CFRP’, Journal of Composites for Construction, vol. 21, no. 1, p. 04016059, 2017.

[14] V. De Luca and C. Marano, ‘Prestressed glulam timbers reinforced with steel bars’, Construction and Building Materials, vol. 30, pp. 206–217, 2012.

[15] W. M. Bulleit, L. B. Sandberg, and G. J. Woods, ‘Steel-reinforced glued laminated timber’, Journal of Structural Engineering, vol. 115, no. 2, pp. 433–444, 1989.

[16] G. Lantos, ‘The flexural behavior of steel reinforced laminated timber beams.’, Wood Science, vol. 2, no. 3, pp. 136–43, 1970.

[17] AS/NZS 1594:2002, Hot-rolled steel flat products. Standards Association of Australia, 2002.

[18] AS 1391:2020, Metallic materials - Tensile testing - Method of test at room temperature. Standards Association of Australia, 2002.

[19] EN 1995, Eurocode 5 Design of Timber Structures. BSI, Brussels, 2004.

[20] Y. De Santis and M. Fragiacomo, ‘Timber-to-timber and steel-to-timber screw connections: Derivation of the slip modulus via beam on elastic foundation model’, Engineering Structures, vol. 244, p. 112798, Oct. 2021, doi: 10.1016/j.engstruct.2021.112798.

[21] G. Schiro, I. Giongo, W. Sebastian, D. Riccadonna, and M. Piazza, ‘Testing of timber-to-timber screw-connections in hybrid configurations’, Construction and Building Materials, vol. 171, pp. 170–186, May 2018, doi: 10.1016/j.conbuildmat.2018.03.078.

[22] A. Ringhofer, ‘Stiffness Properties of Axially Loaded Self-Tapping Screws: 3rd COST FP1402 Workshop’, Mar. 2016.

[23] B. Joachim Hans and S. Yvonne, Steifigkeit axial beanspruchter Vollgewindeschrauben. KIT Scientific Publishing, 2019.

 https://doi.org/10.52202/080513-0307